TRANSACTIONS ON EMERGING TELECOMMUNICATIONS TECHNOLOGIES
Trans. Emerging Tel. Tech. (2016)
Published online in Wiley Online Library (wileyonlinelibrary.com). DOI: 10.1002/ett.3042

RESEARCH ARTICLE

Tri-orthogonal polarization diversity for 5G networks

Nicholas P. Lawrence[1]*, Hedley Hansen[1,2] and Derek Abbott[1]

[1] School of Electrical and Electronic Engineering, The University of Adelaide, SA 5005, Australia
[2] RFT Group EWRD, DSTO, Edinburgh, SA 5111, Australia

ABSTRACT

Millimetre-waves offer the possibility of wide bandwidth and consequently high-data rate for wireless communications. For both uni-polarised and dual-polarised systems, signals sent over a link may suffer severe degradation because of antenna misalignment. Orientation robustness may be enhanced by the use of mutual orthogonality in three dimensions. Multiple-input multiple-output polarisation diversity offers a way of improving signal reception without the limitations associated with spatial diversity. Scattering effects often assist propagation through multipath. However, high-path loss is often considered to limit millimetre-wave propagation, thereby reducing any reception enhancement through scattering. We show that the inclusion of a third orthogonal dipole at a frequency of commercial interest provides antenna orientation robustness in this setting, as well as improved performance in a rich scattering environment, by means of a Ricean fading channel model.

***Correspondence**
Nicholas P. Lawrence, School of Electrical and Electronic Engineering, The University of Adelaide, SA 5005, Australia.
E-mail: nicholas.lawrence@adelaide.edu.au

Received 22 October 2015; Revised 14 February 2016; Accepted 24 March 2016

1. INTRODUCTION

Consumer wireless applications are driving demand for increased user capacity, reliability and throughput. A bottleneck of wireless bandwidth has arisen, leading to interest in frequencies in the millimetre-wave (mmWave) region of the electromagnetic spectrum. Current research of fifth generation (5G) networks is focused on the 28 GHz band, 38 GHz band, 60 GHz band and the E-band (71–76 GHz and 81–86 GHz). Progress in complementary metal–oxide–semiconductor radio frequency integrated circuits is opening up design at mmWave frequencies [1, 2]. In addition to standards defined for indoor wireless personal area networks and wireless local area networks, such as IEEE 802.15.3c [3] and IEEE 802.11ad [4], interest has been stimulated in cellular systems, or outdoor mesh networks [2, 5–7]. Recently, a rate of 7.5 Gbps was announced over a 28 GHz 5G aligned channel in an outdoor setting, a seven-fold increase upon testing results from 18 months earlier [8]. Fifth generation systems may provide both satellite and terrestrial wireless connectivity [9]. Performance should ideally be consistent regardless of end user position and orientation. Multiple-input multiple-output (MIMO) signalling techniques exploiting spatial diversity through channel scattering have been widely adopted in wireless terrestrial applications to increase performance [10–12]. Currently employed systems utilise uni-polarised or dual-polarised propagation because of their ease of implementation. From a simple geometrical analysis, performance is seen to be reliant on relative antenna positions as these types of polarization do not account for a three dimensional environment. Orientation robustness becomes an important limiting factor as design frequency increases to cope with higher data rates. Every possible design advantage needs to be sought.

Innovative design at mmWave frequencies offers many of the advantages of both microwave and terahertz frequencies while minimising the disadvantages [13]. Firstly, a large bandwidth of up to 7 GHz within the mmWave spectrum has been allocated to wireless design over short distances [14]. This supports high-data rate using low order modulation techniques, such a binary phase shift keying and so provides propagation robustness in the case of perfect alignment. Secondly, design and implementation may be influenced by well documented microwave techniques. Thirdly, available power at these frequencies does not necessarily restrict the system to line of sight (LoS) propagation [15].

Dual polarisation has been seen to enhance capacity in a LoS communication environment where relative transmitter–receiver antenna alignment varies with relative position [16, 17]. A dual-polarised antenna may be represented as a combination of two propagating orthogonal linear dipoles. In effect, this combination allows all forms of elliptically polarised waveform, including circularly polarised waveforms, to be transmitted and received [18].

Such an antenna is optimised in the broadside direction, orthogonal to the antenna surface. Suboptimal performance occurs when a transmit antenna or receive antenna is not aligned in the direction of propagation between them.

Inclusion of a third orthogonal dipole at the antenna, leading to a tri-orthogonal configuration, enhances performance beyond that of a dual-polarised system by mitigating antenna misalignment [19, 20]. Theoretically, capacity is maintained in any given direction as dual polarisation is offered over all unit vector directions. In the instance of LoS propagation, polarisation diversity offers the benefit of MIMO signalling techniques that is not always the case for a spatially diverse system. An arrangement of three dipoles, at the antenna, may provide yet greater capacity if the orthogonality criteria between dipoles is relaxed [21]. However, this arrangement does not optimise capacity for all propagation directions in a field-of-view (FoV) in which all antenna orientations are observed.

The benefit of a rich scattering environment enhances system performance [11] and is often cited in reference papers pertaining to MIMO systems [19, 20, 22]. Such an environment is location dependent and typically occurs in urbanised areas at 28 GHz [13].

A wireless channel is a time-varying combination of a LoS signal together with a non-line of sight (NLoS) component arising from the channel environment and multipath. Relative transmitter–receiver motion may be introduced. Because of orthogonality, the electric field orientations of the propagating electromagnetic signals are affected independently, reducing correlation which, together with any variation in the channel environment, presents many ways for a signal to arrive at the receiver. As a result, throughput may be enhanced through no additional transmit power and little additional processing. Deriving full benefit over any channel is reliant on a precise alignment of transmit and receive antennas.

Performance of links employing tri-orthogonal antenna configurations has been shown to be less sensitive to orientation and antenna misalignment, providing diversity gain and increased capacity in rich scattering environments [19, 20, 23]. Compact tri-orthogonal antennas are present at lower microwave frequencies, which rely on differential feeding, and are capable of beamsteering through phasing techniques to increase performance in a given vector direction [24]. At the receiver, MIMO detection and interference cancellation are feasible because of the tri-orthogonal arrangement, provided that transmitter signalling and receiver processing account for radio wave polarisation according to link geometry at the receiver location. Polarisation-time code signalling is practicable [25, 26].

In this paper, we propose a channel model with a fundamental physical approach. The model incorporates wireless link geometry in addition to polarisation mismatch, and a tri-orthogonal transmit and receive antenna at either end of the link. Furthermore, this paper analyses whether a tri-orthogonal system provides channel capacity enhancement through all possible antenna orientations.

2. METHODS

To understand the benefits of polarisation in three dimensions, we look to spherical geometry, used in satellite communications design [27, 28].

We assume three mutually orthogonal unit dipole antennas at both transmitter and receiver. These excite and respond to the polarised signal in three dimensions. All unit dipoles are half-wavelength ($\lambda/2$) in length.

The FoV and relevant nomenclature are now introduced. In Figure 1, the receiver R is observed to move upon a spherical surface. This surface introduces both variable path length and orientation. The outer radius of the FoV is the point at which transmitter T is at the horizon of R. As the FoV is circular, all orientations of the proposed antenna system configuration are included in the FoV. 33333

Referring to Figure 2, at T, unit dipole $\hat{\mathbf{x}}$ is aligned with the positive A axis, coinciding with an azimuthal angle θ_T, as observed from T, of 0°. Unit dipole $\hat{\mathbf{y}}$ is aligned with the positive B axis, coinciding with an azimuthal angle θ_T of 90°. Unit dipole $\hat{\mathbf{z}}$ is aligned with the positive C axis.

At R, and at the FoV centre, unit dipole $\hat{\mathbf{p}}$ is parallel to the A axis, coinciding with an azimuthal angle θ_T of 0π radians, or 0°. Unit dipole $\hat{\mathbf{q}}$ is parallel to the B axis, coinciding with an azimuthal angle θ_T of 0.5π radians, or 90°. Unit dipole $\hat{\mathbf{r}}$ is a radial unit dipole aligned with the C axis.

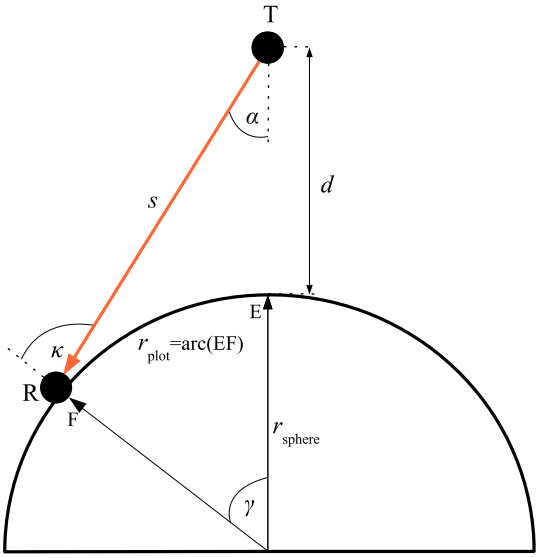

Figure 1. Link geometry: the receiver R is positioned on a semicircle determined by simple geometry. The proximal distance between transmitter T and R is d, s is path length while angles α, κ and γ are used to determine relative position. The entire system is rotated about the field-of-view (FoV) centre by 360° to develop a spherical surface, forming the FoV. The number of concentric paths on the sphere together with the azimuthal step increment about the FoV centre is set by the user. The algorithm begins at the FoV centre and works out to the circular path where κ = 90°.

DOI: 10.1002/ett

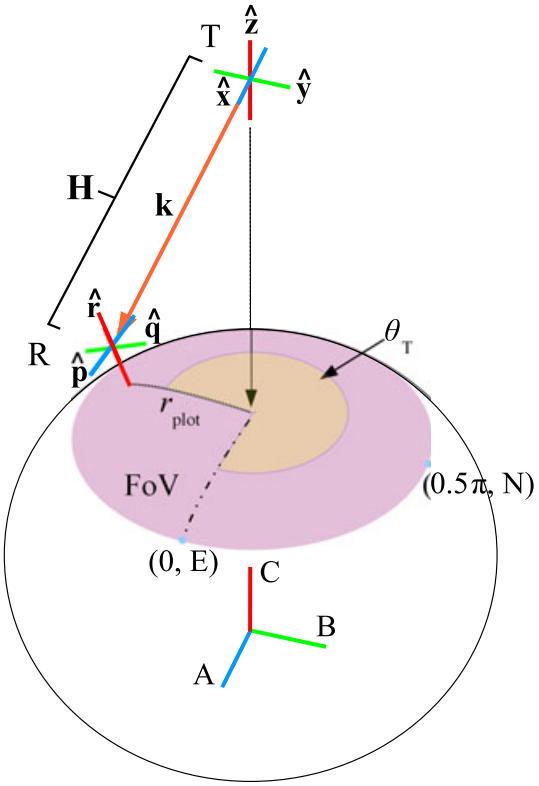

Figure 2. System according to specific location in the field-of-view (FoV): the propagation vector, **k**, is unique to any position in the FoV, and is given according to the azimuthal angle θ_T and the radial distance from the FoV centre, r_{plot}. Easterly and northerly directions simplify description of the movement of R in the FoV. Unit dipole orientations at R are calculated according to Equations (8–(10), in three dimensional space. These, along with the static unit dipole orientations, at T, of $\hat{\mathbf{x}}$, $\hat{\mathbf{y}}$ and $\hat{\mathbf{z}}$, then permit the determination of the parametres required to analyse the channel, **H**, as a function of FoV location.

To effectively explain movement of R within the FoV, easterly and northerly compass directions are invoked, corresponding to azimuthal angles of θ_{T} of 0° and 90° respectively. In Figure 2, unit dipole $\hat{\mathbf{p}}$ is deemed to be aligned in an easterly direction, while unit dipole $\hat{\mathbf{q}}$ is deemed to be aligned in a northerly direction, for any position of R in the FoV. Unit dipole $\hat{\mathbf{r}}$ is aligned orthogonally to unit dipoles $\hat{\mathbf{p}}$ and $\hat{\mathbf{q}}$.

Link geometry is determined according to Figure 1 and to the following equations,

$$\gamma = \frac{r_{\text{plot}}}{r_{\text{sphere}}} \tag{1}$$

$$s = \sqrt{u^2 + r_{\text{sphere}}^2 - 2ur_{\text{sphere}}\cos\gamma} \tag{2}$$

$$\kappa = \arcsin\left(\frac{u}{s}\sin\gamma\right) \tag{3}$$

$$\alpha = \arcsin\left(\frac{u}{s}\sin\gamma\right) - \gamma \tag{4}$$

$$\gamma_{\max} = \arccos\left(\frac{r_{\text{sphere}}}{u}\right) \tag{5}$$

$$s_{\max} = u\cos\alpha \tag{6}$$

$$\alpha_{\max} = \arcsin\left(\frac{r_{\text{sphere}}}{u}\right) \tag{7}$$

where u is $r_{\text{sphere}} + d$.

Observing from T, counter clockwise rotation about the positive C axis looking toward the FoV is deemed positive, as in Figure 2. Elevation at T is given by α with 0° in the negative C axis direction, otherwise positive. Elevation at the receiver is given by κ, with 0° in the positive C axis direction at the FoV centre, otherwise positive.

To describe orientation of the six dipoles, a set of right-handed Cartesian axes is invoked, as per Figure 2. Axes A, B and C are used to describe receiver position on the sphere surface. Lengths a, b and c are along these axes, repectively, and are normalised by r_{sphere}. The unit vectors representing unit dipoles $\hat{\mathbf{x}}$, $\hat{\mathbf{y}}$, $\hat{\mathbf{z}}$ and $\hat{\mathbf{r}}$, are respectively $\hat{\mathbf{x}} = [100]^{\text{T}}$, $\hat{\mathbf{y}} = [010]^{\text{T}}$, $\hat{\mathbf{z}} = [001]^{\text{T}}$ and,

$$\hat{\mathbf{r}} = \begin{bmatrix} \cos\theta_{\text{T}}\sin\gamma \\ \sin\theta_{\text{T}}\sin\gamma \\ \cos\gamma \end{bmatrix} \tag{8}$$

where the superscript T denotes transpose.

The position on the spherical surface, relative to the FoV centre position, must be known to describe the orientation of dipoles $\hat{\mathbf{p}}$ and $\hat{\mathbf{q}}$,

$$\hat{\mathbf{p}} = \begin{bmatrix} \cos(\text{atan}_2(a,c)) \\ 0 \\ -\sin(\text{atan}_2(a,c)) \end{bmatrix} \tag{9}$$

$$\hat{\mathbf{q}} = \begin{bmatrix} -\sin(\arcsin(b))\sin(\text{atan}_2(a,c)) \\ \cos(\arcsin(b)) \\ -\sin(\arcsin(b))\cos(\text{atan}_2(a,c)) \end{bmatrix} \tag{10}$$

where $\text{atan}_2(a,c)$ is described as,

$$\text{atan}_2(a,c) = \begin{cases} \arctan(\frac{a}{c}) & (c \succ 0) \\ \arctan(\frac{a}{c}) + \pi & (a \succeq 0, c \prec 0) \\ \arctan(\frac{a}{c}) - \pi & (a \prec 0, c \prec 0) \\ +\pi/2 & (a \succ 0, c = 0) \\ -\pi/2 & (a \prec 0, c = 0) \\ \text{undefined} & (a = 0, c = 0) \end{cases} \tag{11}$$

At the FoV centre in Figure 2, $a = 0$, $b = 0$, and $c = 1$. A unit propagation vector, $\hat{\mathbf{k}}$, is given as,

$$\hat{\mathbf{k}} = \begin{bmatrix} \cos\theta_{\mathrm{T}} \sin\alpha \\ \sin\theta_{\mathrm{T}} \sin\alpha \\ -\cos\alpha \end{bmatrix} \tag{12}$$

The azimuthal angle θ_R, at R, in the FoV at a position given by the unit propagation vector $\hat{\mathbf{k}}$, differs from the corresponding angle θ_T, at T, by 180°. The receiver R is assumed to be at a distance s, from T, that varies according to FoV location. Ideally, power transfer over the FoV is high and constant. The possibility of high capacity communication in any unit vector direction can be evaluated. Where deep fading is encountered, diversity, through redundancy, may be introduced [26, 29]. An ideal channel is one where recourse to this is kept to a minimum.

Power transfer between a unit dipole at T and at R is borne out through the Friis formula [18, 30]. For a mutually tri-orthogonal antenna transmitter and receiver, nine sub-channel paths are generated. The Friis formula is given as

$$\frac{P_{\mathrm{R}}}{P_{\mathrm{T}}} = G_{\mathrm{T}}(\phi_T, \theta_T) G_{\mathrm{R}}(\phi_R, \theta_R) \left(\frac{\lambda}{4\pi s}\right)^2 e_{\mathrm{pol}} L_{\mathrm{atmos}} \tag{13}$$

where R refers to the receiver, T refers to the transmitter, P is power, G is dipole gain, λ is transmitted wavelength, s is separation of transmitter and receiver, e_{pol} is the polarisation mismatch between the two dipoles and L_{atmos} is atmospheric attenuation at 28 GHz and is given here as 0.06 dBkm^{-1} [13]. The angles ϕ and θ are elevation and azimuth angles, respectively.

The power gain G of a half-wavelength dipole is given by Equation (14) [18, 30, 31]. This assumes 100 % dipole efficiency and is given as,

$$G(\theta, \phi) = \frac{1.64}{\sin^2\phi} \cos^2\left(\frac{\pi}{2}\cos\phi\right). \tag{14}$$

In the case of unit dipole $\hat{\mathbf{z}}$ at T, angle ϕ is represented by α, as shown in Figure 1. At T, minimum gain is when α is 0°. Maximum gain is when α is 90°, which is not in the FoV. We note that the gain of unit dipole $\hat{\mathbf{z}}$ is independent of the azimuthal angle θ_T. In this paper, the gain profiles of transmit dipoles $\hat{\mathbf{x}}$ and $\hat{\mathbf{y}}$ are masked with a gain profile of 24 dB over the FoV [13, 32].

In the case of unit dipole $\hat{\mathbf{r}}$ at R, angle ϕ is represented by κ, the sum of α and γ, as in Figure 1. For unit dipoles $\hat{\mathbf{p}}$ and $\hat{\mathbf{q}}$, angle ϕ is determined by considering the inner product of the unit dipole vector and the unit propagation vector $\hat{\mathbf{k}}$, with κ replacing ϕ in Equation (14). Figure 3 shows gain profiles of the half-wavelength dipoles, $\hat{\mathbf{z}}$, $\hat{\mathbf{p}}$, $\hat{\mathbf{q}}$ and $\hat{\mathbf{r}}$.

A signal may incur polarisation mismatch loss over a link when two antennas do not have their polarisations perfectly aligned [30, 31]. Polarisation mismatch, e_{pol}, may be determined for any unit dipole pair. For the unit dipole pair

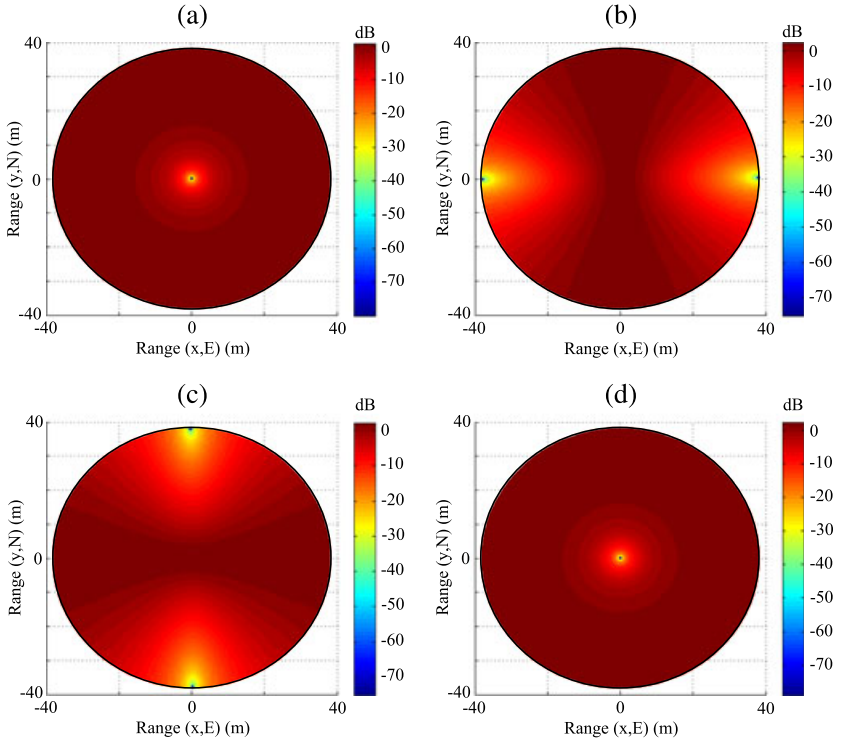

Figure 3. Gain (G) (dB) profiles of the unit half-wavelength dipoles over an field-of-view described by a propagation distance of 10 m, and spherical radius of 81 m: (a) $G_{\hat{\mathbf{z}}}$, (b) $G_{\hat{\mathbf{p}}}$, (c) $G_{\hat{\mathbf{q}}}$ and (d) $G_{\hat{\mathbf{r}}}$. The gain profiles of dipoles $\hat{\mathbf{x}}$ and $\hat{\mathbf{y}}$ at T are masked with a gain profile of 24 dB over the FoV [13, 32].

DOI: 10.1002/ett

$\hat{\mathbf{r}}\hat{\mathbf{z}}$, the polarisation mismatch may be given by the inner product in Equation (15),

$$e_{\text{pol}(\hat{\mathbf{r}}\hat{\mathbf{z}})} = |\hat{\mathbf{r}}_{\perp\mathbf{k}} \cdot \hat{\mathbf{z}}_{\perp\mathbf{k}}|^2 \tag{15}$$

where $\hat{\mathbf{r}}_{\perp\mathbf{k}}$ and $\hat{\mathbf{z}}_{\perp\mathbf{k}}$ are projections onto the plane perpendicular to the unit propagation vector $\hat{\mathbf{k}}$.

The projection of an arbitrary vector $\mathbf{v}$ onto the plane perpendicular to $\hat{\mathbf{k}}$ may be given by

$$\mathbf{v}_{\perp\mathbf{k}} = \left(\mathbf{I}_3 - \hat{\mathbf{k}}\hat{\mathbf{k}}^{\mathrm{T}}\right)\hat{\mathbf{v}}, \tag{16}$$

which can then normalised to give,

$$\hat{\mathbf{v}}_{\perp\mathbf{k}} = \frac{\mathbf{v}_{\perp\mathbf{k}}}{|\mathbf{v}_{\perp\mathbf{k}}|}. \tag{17}$$

Polarisation mismatch profiles are given in Figure 4 for all unit dipole pair combinations. Received symbols may be given according to Goldsmith (2005) [11] and Equation (21) where,

$$\mathbf{Y} = \mathbf{H}\mathbf{X} + \mathbf{N}. \tag{18}$$

In Equation (21), $\mathbf{Y}$ is the set of received signals at the receiver, $\mathbf{H}$ represents a 3×3 complex fading channel matrix, $\mathbf{X}$ is a block of symbols sent and $\mathbf{N}$ is complex additive white Gaussian noise (AWGN) at the receiver R.

The complex fading channel matrix may be decomposed into the sum of an average LoS component ($\bar{\mathbf{H}}$) and a variable scattered NLoS component ($\tilde{\mathbf{H}}$) given by,

$$\mathbf{H} = \sqrt{\frac{K}{1+K}}\bar{\mathbf{H}} + \sqrt{\frac{1}{1+K}}\tilde{\mathbf{H}} \tag{19}$$

where K is the Ricean K-factor [11]. Note that $K = 0$ corresponds to a pure Rayleigh fading channel, while

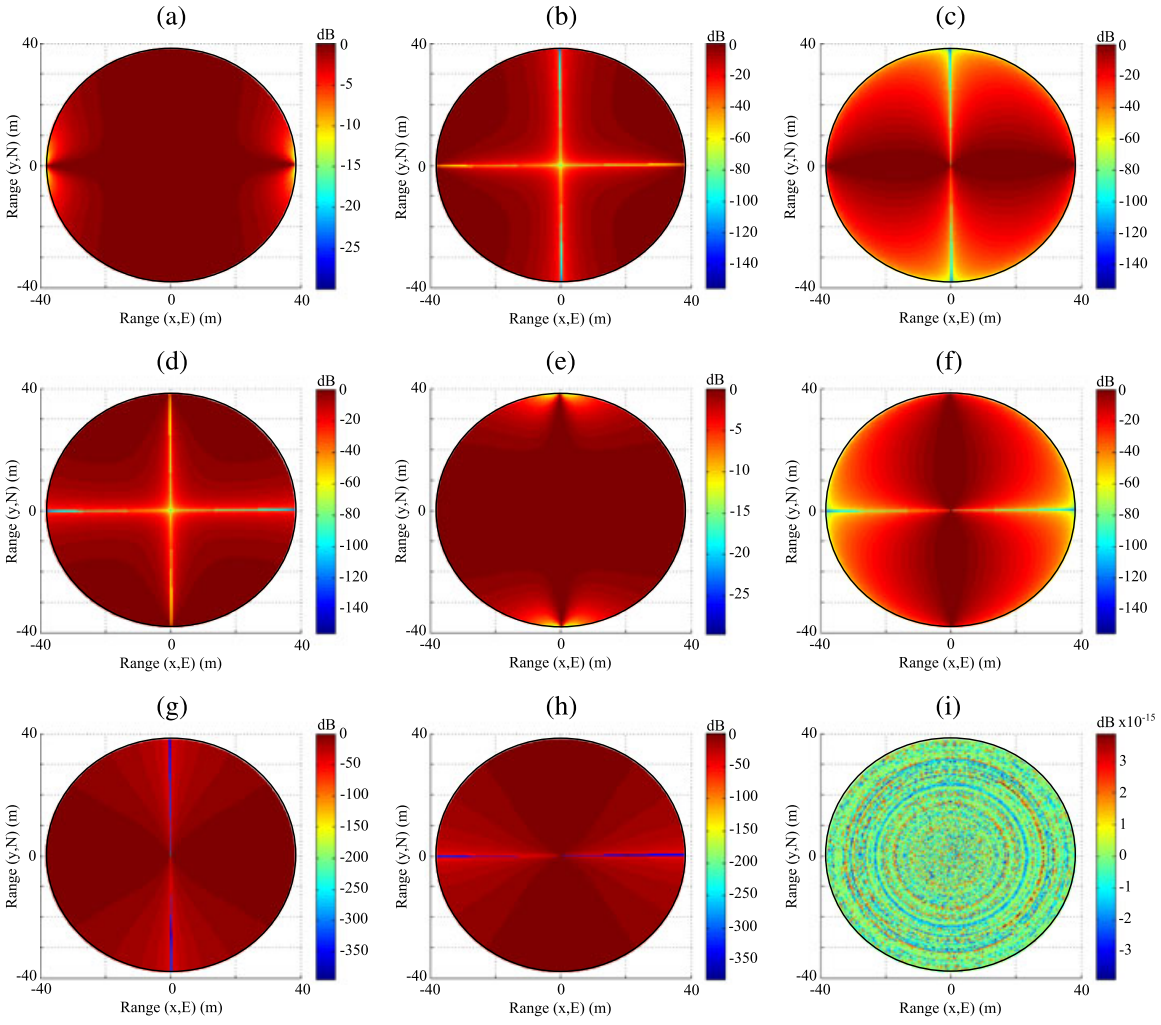

Figure 4. Polarisation mismatch (e_{pol}) (dB) profiles for each unit dipole pair over a field-of-view described by a propagation distance of 10 m, and spherical radius of 81m: (a) $\hat{\mathbf{p}}\hat{\mathbf{x}}$, (b) $\hat{\mathbf{p}}\hat{\mathbf{y}}$, (c) $\hat{\mathbf{p}}\hat{\mathbf{z}}$, (d) $\hat{\mathbf{q}}\hat{\mathbf{x}}$, (e) $\hat{\mathbf{q}}\hat{\mathbf{y}}$, (f) $\hat{\mathbf{q}}\hat{\mathbf{z}}$, (g) $\hat{\mathbf{r}}\hat{\mathbf{x}}$, (h) $\hat{\mathbf{r}}\hat{\mathbf{y}}$, (i) $\hat{\mathbf{r}}\hat{\mathbf{z}}$.

$K = \infty$ corresponds to a pure AWGN fading channel or LoS system.

Without loss of generality, we assume the phase argument of the AWGN fading channel coefficient to be zero. The LoS power transfer for each unit dipole pair, given by Equation (13), forms a basis to determine the channel coefficients in Equation (20), unique to a FoV location. These coefficients are obtained from $\sqrt{P_R/P_T}$. The polarisation mismatch factor, e_{pol}, includes projections via Equation (16), with the 3×3 matrix $\mathbf{H}$ being at most rank 2 in the LoS case. Channel rank, and therefore capacity, may be increased via multipath fading [11].

Applications of the channel model, in the AWGN fading or LoS case, are currently restricted and may include an improved determination of the LoS component used for channel state information to optimise transmission. Use of omnidirectional antennas enhances multipath in the case of a Rayleigh fading channel, increasing capacity over the FoV. Doppler frequency shift, caused by relative transmitter–receiver motion, is omitted, as are near-field and correlation effects. The channel $\mathbf{H}$ may be given as,

$$\mathbf{H} = \begin{bmatrix} h_{\hat{\mathbf{p}}\hat{\mathbf{x}}} & h_{\hat{\mathbf{p}}\hat{\mathbf{y}}} & h_{\hat{\mathbf{p}}\hat{\mathbf{z}}} \\ h_{\hat{\mathbf{q}}\hat{\mathbf{x}}} & h_{\hat{\mathbf{q}}\hat{\mathbf{y}}} & h_{\hat{\mathbf{q}}\hat{\mathbf{z}}} \\ h_{\hat{\mathbf{r}}\hat{\mathbf{x}}} & h_{\hat{\mathbf{r}}\hat{\mathbf{y}}} & h_{\hat{\mathbf{r}}\hat{\mathbf{z}}} \end{bmatrix} \tag{20}$$

where the matrix coefficients in equation (20) represent signal transfer between a unit dipole pair. The channel $\mathbf{H}$ may be calculated for any position in the FoV.

Capacity for M receivers and N transmitters is given according to Equation (21)[25, 26, 33] as,

$$C = \log_2 \left| \left(\mathbf{I}_M + \frac{\rho}{\mathrm{N}} \mathbf{H}\mathbf{H}^{\dagger} \right) \right| \tag{21}$$

where $\mathbf{I}$ represents an identity matrix, ρ the average signal-to-noise ratio and † denotes the Hermitian transpose.

3. RESULTS

We present simulated three dimensional results covering all possible orientations between T and R over a FoV using system parametres in [32]. We simulate with an operating frequency of 28 GHz, a bandwidth of 250 MHz, gain pro-

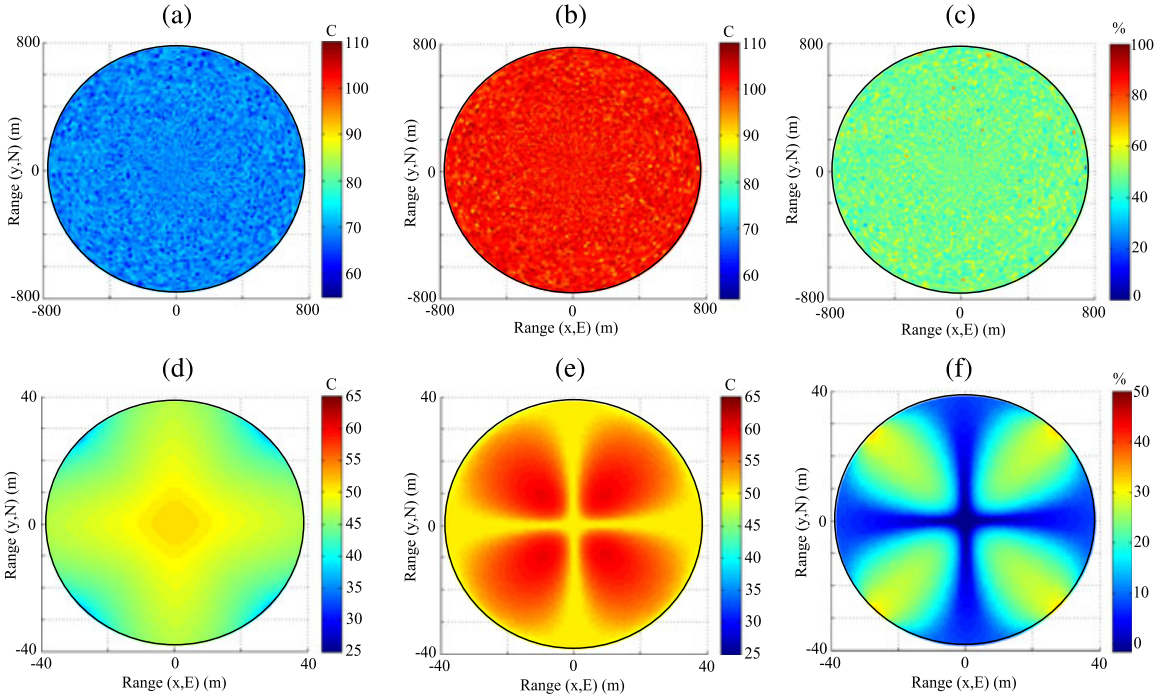

Figure 5. Capacity over the field-of-view (FoV): (a) typical urban mmWave fading channel capacity over the FoV, as produced by a dual-polarised antenna at each end of the link (2×2 arrangement), (b) shows a typical urban mmWave fading channel capacity over the FoV, as produced by a tri-orthogonal antenna at each end of the link (3×3 arrangement), (c) typical urban mmWave fading channel capacity advantage over the FoV, presented as a percentage, as produced by replacing the dual-polarised antenna with a tri-orthogonal antenna at each end of the link, (d) additive white Gaussian noise (AWGN) fading channel capacity over the FoV,as produced by a dual-polarised antenna at each end of the link (2×2 arrangement), (e) AWGN fading channel capacity over the FoV, as produced by a tri-orthogonal antenna at each end of the link (3×3 arrangement), (f) AWGN fading channel capacity advantage over the FoV, presented as a percentage, as produced by replacing the dual-polarised antenna with a tri-orthogonal antenna at each end of the link.

files as described in Section 2, a transmit power of 29 dBm, a system noise temperature of 290 K and mutual dipole coupling of 0.3 [34]. For the first scenario, we consider a propagation distance at the FoV centre of 200 m, with a spherical radius of 1620 m, thus defining all possible orientations. A channel exponent of 3.53 [32, 35] and a Ricean K-factor of K=10, typical of an urban mmWave channel [36, 37] are employed. The results are shown in Figures 5 (a–c). For the second scenario, we consider a propagation distance at the FoV centre of 10 m, and a spherical radius of 81 m, thus defining all possible orientations. A channel exponent of 1.68 [13, 35], and a Ricean K-factor of K=∞, correspond to a LoS environment. The results are shown in Figures 5 (d–f).

Figure 5 shows capacity in the FoV resulting from dual-polarised and tri-orthogonal signal propagation over an urban mmWave channel and a AWGN fading channel. In Figure 5(c), the inclusion of a simple omnidirectional half-wavelength dipole at T and R, orthogonal to the dual polarisations of a typical patch antenna, is able to provide an improved capacity over the majority of the FoV, typically of the order of 50%. In effect, a quasi-Rayleigh channel (K=10) provides multipath enhancement regardless of antenna orientation. This is seen by the quasi-homogeneity over the FoV in Figures 5(a) and (b). For such a channel, the additional of the third orthogonal dipole provides an increase in capacity, rather than orientation robustness.

We note in Figure 5(f) that the inclusion of a simple omnidirectional half-wavelength dipole at the T and R, orthogonal to the dual polarisations of a typical patch antenna, is able to provide an improved capacity over the majority of the FoV. We note a small decrease in performance at the FoV centre, but as this is the position of maximum capacity for the 2×2 system (Figure 5(d)), corresponding to the instance of perfect alignment, this may be considered as a small compromise for enhanced performance over the remainder of the FoV. Whereas a 2×2 system provides a peak capacity at the FoV centre, capacity for the 3×3 system in an AWGN channel is seen to be highest at four offset positions approximately 20° off-centre and at 45°, 135°, 215° and 305° azimuth (Figure 5(e)). This is suggestive of orientation robustness in the absence of a scattering mechanism.

4. DISCUSSION

The analysis provided in this paper suggests that orientation robustness at 28 GHz over a 5G wireless channel is provided by inclusion of a simple third orthogonal half-wavelength dipole in both transmitter and receiver design, providing a tri-orthogonal arrangement at both ends of a link. The analysis covers two extreme channel cases that of a short-range LoS indoor environment and also that of a longer range urban mmWave or NLoS outdoor environment. The analysis is based on test system parametres. Compact tri-orthogonal antenna design exists at lower frequencies, and its implementation at mmWave frequencies would provide orientation robustness for 5G systems, regardless of location. With the assistance of a channel providing multipath effects, such as an urban channel, we observe that the third orthogonal dipole may provide an improvement in system performance through increased capacity, regardless of antenna orientation.

REFERENCES

1. Doan C, Emami S, Sobel D, Niknejad A, Brodersen RW. Design considerations for 60 GHz CMOS radios. *IEEE Communications Magazine* 2004; **42**(12): 132–140. DOI: 10.1109/MCOM.2004.1367565.
2. Rappaport T, Murdock J, Gutierrez F. State of the art in 60-GHz integrated circuits and systems for wireless communications. *Proceedings of the IEEE* 2011; **99**(8): 1390–1436. DOI: 10.1109/JPROC.2011.2143650.
3. IEEE. IEEE 802.15 WPAN task group 3c (TG3c) millimeter wave alternative PHY, 2009. Available from: http://www.ieee802.org/15/pub/TG3c.html [July 2015].
4. IEEE. Draft standard for information technology telecommunications and information exchange between systems local and metropolitan area networks specific requirements part 11: wireless LAN medium access control (MAC) and physical layer (PHY) specifications-amendment 3: Enhancements for very high throughput in the 60 GHz band, 2012. Available from: http://ieeexplore.ieee.org/xpl/mostRecentIssue.jsp?punumber=6242353 [July 2015].
5. Pietraski P, Britz D, Roy A, Pragada R, Charlton G. Millimeter wave and terahertz communications: feasibility and challenges, 2012. Available from: http://wwwen.zte.com.cn/endata/magazine/ztecommunications/2012/4/articles/201301/t20130106_380442.html [July 2015].
6. Rangan S, Rappaport T, Erkip E. Millimeter-wave cellular wireless networks: potentials and challenges. *Proceedings of the IEEE* 2014; **102**(3): 366–385. DOI: 10.1109/JPROC.2014.2299397.
7. Pi Z, Khan F. An introduction to millimeter-wave mobile broadband systems. *IEEE Communications Magazine* 2011; **49**(6): 101–107. DOI: 10.1109/MCOM.2011.5783993.
8. Samsung Electronics Inc. *Samsung Electronics sets 5G speed record at 7.5 Gbps, over 30 times faster than 4G LTE*, 2014. Available from: http://www.samsung.com/uk/news/local/samsung-electronics-sets-5g-speed-record-at-7-5gbps-over-30-times-faster-than-4g-lte [July 2015].
9. Mak KM, Lai HW, Luk KM, Chan CH. Circularly polarized patch antenna for future 5G mobile phones. *IEEE Access* 2014; **2**: 1521–1529. DOI: 10.1109/ACCESS.2014.2382111.

10. Jakes W. *Microwave Mobile Communications*. Wiley: New York, NY, 1974.
11. Goldsmith A. *Wireless Communications*. Cambridge University Press: Cambridge, UK, 2005.
12. Paulraj A, Gore D, Nabar R, Bolcskei H. An overview of MIMO communications–a key to gigabit wireless. *Proceedings of the IEEE* 2004; **92**(2): 198–218. DOI: 10.1109/JPROC.2003.821915.
13. Rappaport T, Sun S, Mayzus R, Zhao H, Azar Y, Wang K. *et al*. Millimeter wave mobile communications for 5G cellular: it will work! *IEEE Access* 2013; **1**: 335–349. DOI: 10.1109/ACCESS.2013.2260813.
14. Rappaport T. The coming renaissance of the wireless communications age, 2014. Available from: http://wireless.engineering.nyu.edu/presentations/NYSWAX.pdf [May 2015].
15. Plextek RF Integration Ltd. A 4-channel 28 GHz power amplifier with 4-bit digital phase control for 5G RF front ends 2015. Available from: http://www.plextekrfi.com/wp-content/uploads/5g_28GHz_PA_PS.pdf [October 2015].
16. Arapoglou P, Liolis K, Bertinelli M, Panagopoulos A, Cottis P, De Gaudenzi R. MIMO over satellite: a review. *IEEE Communications Surveys Tutorials* 2011; **13**(1): 27–51. DOI: 10.1109/SURV.2011.033110.00072.
17. Nabar R, Bolcskei H, Erceg V, Gesbert D, Paulraj A. Performance of multiantenna signaling techniques in the presence of polarization diversity. *IEEE Transactions on Signal Processing* 2002; **50**(10): 2553–2562.
18. Pozar D. *Microwave Engineering* (4th edition). John Wiley and Sons: New York, 2011.
19. Chiu CY, Yan JB, Murch RD. Compact three-port orthogonally polarized MIMO antennas. *IEEE Antennas and Wireless Propagation Letters* 2007; **6**: 619–622, DOI: 10.1109/LAWP.2007.913272.
20. Andrews M, Mitra P, de Carvalho R. Tripling the capacity of wireless communications using electromagnetic polarization. *Nature*; **409**: 316–318, DOI: 10.1038/35053015.
21. Valenzuela-Valdes J, Garcia-Fernandez M, Martinez-Gonzalez A, Sanchez-Hernandez DA. Evaluation of true polarization diversity for MIMO systems. *IEEE Transactions on Antennas and Propagation* 2009; **57**(9): 2746–2755.
22. Shafi M, Zhang M, Moustakas A, Smith P, Molisch A, Tufvesson F, *et al*. Polarized MIMO channels in 3-D: models, measurements and mutual information. *IEEE Journal on Selected Areas in Communications* 2006; **24**(3): 514–527, DOI: 10.1109/JSAC.2005.862398.
23. Horvath P, Frigyes I. Sat02-6: Application of the 3D polarization concept in satellite MIMO systems. In *IEEE Global Telecommunications Conference (GLOBECOM '06)*, San Francisco, USA, 2006; 1–5, DOI: 10.1109/GLOCOM.2006.481.
24. Zou L, Fumeaux C. A cross-shaped dielectric resonator antenna for multifunction and polarization diversity applications. *IEEE Antennas and Wireless Propagation Letters* 2011; **10**: 742–745, DOI: 10.1109/LAWP.2011.2162479.
25. Proakis J. *Digital Communications*. McGraw Hill: New York, 2001.
26. Paulraj A, Nabar R, Gore D. *Introduction to Space-time Wireless Communications*. Cambridge University Press: Cambridge, UK, 2003.
27. Ryan M. *Principles of satellite communications*. Argos Press Series in Telecommunications Systems: Argos Press Pty. Ltd., Canberra, Australia, 2003.
28. Roddy D. *Satellite Communications, Fourth Edition (Professional Engineering)*. McGraw-Hill Professional: New York, 2006.
29. Adve R. *Receive diversity*, 2008. Available from: http://www.comm.toronto.edu/ rsadve/Notes/DiversityReceive.pdf [July 2015].
30. Orfanidis S. *Electromagnetic Waves and Antennas Book*. Rutgers University Press: NJ, USA, 2002. Available from: http://www.ece.rutgers.edu/faculty/orfanidis [July 2015].
31. Balanis C. *Antenna Theory: Analysis and Design*. J.Wiley and Sons Inc.: New York, NY, 1997.
32. Samsung Electronics Inc. Samsung 5G vision, 2015. Available from: http://www.samsung.com/global/business-images/insights/2015/Samsung-5G-Vision-0.pdf [July 2015].
33. Bohagen F, Orten P, Oien G. Construction and capacity analysis of high-rank line-of-sight MIMO channels. In *IEEE Wireless Communications and Networking Conference*, New Orleans, USA, 2005; **1**:432–437, DOI: 10.1109/WCNC.2005.1424539.
34. Sirianunpiboon S, Howard S, Calderbank A, Davis L. Fully-polarimetric MIMO to improve throughput and reliability across propagation conditions. In *IEEE 70th Vehicular Technology Conference Fall (VTC 2009-Fall)*, Anchorage, USA, 2009; 1–5, DOI: 10.1109/VETECF.2009.5379016.
35. Wang J, Zhang H, Tingting L, Gulliver T. Capacity of 60 GHz wireless communication systems over fading channels. *Journal of Networks* 2012; **7**(1): 203–209. DOI: 10.4304/JNW.7.1.203-209.
36. Baek S, Chang Y, Hur S, Hwang J, Kim B. 3-Dimensional large-scale channel model for urban environments in mmwave frequency. In *IEEE International Conference on Communication Workshop (ICCW)*, London, UK, 2015; 1220–1225, DOI: 10.1109/ICCW.2015.7247344.
37. University of South Wales. mmWave 28, 40 and 60 GHz RF modelling for small cells, 5G mobile networks and WiGig applications, 2015. Available from: http://woric.research.southwales.ac.uk/mmwave_model/.